UAV Gust Wind Mitigation Measurement and Control System Design

Yingjian Lu
School of Electronic and Information Engineering
Beihang University
Beijing, China
luyingjian@buaa.edu.cn

Chunhui Liu
Institute of Unmanned system
Beihang University
Beijing China
liuchunhui2134@buaa.edu.cn

***Abstract*—UAVs are susceptible to turbulence when flying, which can alter the expected navigational attitude, flight trajectory and other states and affect the reasonable execution of the mission, and gust mitigation technology is a powerful means for UAVs to cope with the effects of gusts. This paper designs a gust mitigation measurement and control system for UAVs using the STM32H743 as the control core. The system consists of a master control unit, a data acquisition module, a serial module, a rudder control module and a data storage module. When the UAV is affected by gusts of wind, the system acquires the current flight status of the UAV by accurately collecting data from the UAV sensors, and then combines the control commands from the ground station and the flight control to fuse and solve the data, and then generates rudder control commands to control the rudder deflection, so that the UAV can maintain stable flight and achieve gust mitigation. After actual circuit fabrication and experimental testing, the measurement and control system designed in this paper can achieve stable serial communication, accurate analogue signal acquisition, precise motor and rudder control and stable power supply, meeting all the indicators and requirements required to achieve gust mitigation.**

Keywords—UAV, gust mitigation, circuit design

I. INTRODUCTION

With the rapid development of Unmanned Aerial Vehicle (UAV) related technologies, UAVs are playing an increasingly important role in many fields. UAVs are now capable of performing a variety of tasks such as remote sensing, filming, mapping, rescue, and surveillance [1]. With the increasing level of autonomy of UAVs, their control methods have also developed from simple remote control or program control to the level of autonomous control, which has put forward higher requirements for UAV flight control systems. However, UAVs are susceptible to bumps during flight by turbulence [2,3], thus changing the expected attitude, trajectory and other states, affecting the reasonable execution of work tasks and even causing more serious consequences.

Gust mitigation control can effectively reduce various dynamic responses (including center-of-mass overload, wingtip overload, wing root bending moment, wing deformation, etc.) of the aircraft under gust excitation, thus ensuring the flight safety of the aircraft [4]. In the field of engineering applications, gust mitigation can be carried out passively through targeted wing structure optimization design, such as deformed wings [5,6], wingtip winglets [7], etc.; it can also be carried out actively through active control techniques, and active gust mitigation based on the conventional control surfaces of the aircraft is a relatively more mature and reliable way. By driving the aircraft rudder deflection to offset the additional aerodynamic forces caused by the gusts, the gust mitigation purpose is achieved [8].

This work was supported by the Science and Technology Innovation 2030-Key Project of "New Generation Artificial Intelligence" under Grant 2020AAA0108200.

Based on this background, this paper develops an STM32-based UAV gust mitigation measurement and control system for UAV gust mitigation needs, then describes the hardware and software design of the system, and finally conducts experimental testing and analysis of the four modules of the system.

II. OVERALL SYSTEM DESIGN

The UAV gust wind mitigation measurement and control system consists of a master control unit, a data acquisition module, a serial module, a rudder control module, and a data storage module, and the hardware structure of the system is shown in Fig. 1. The system hardware structure is shown in Fig. 1. The red boxes are the external devices to be connected to the system.

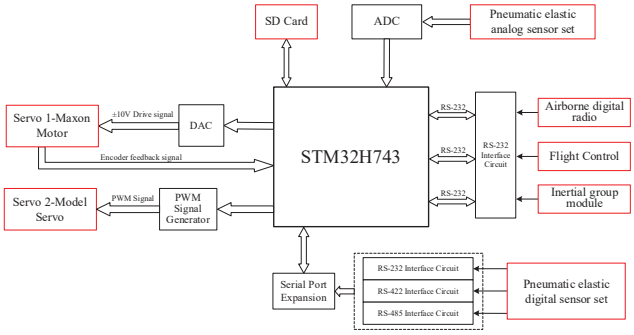

Fig. 1. UAV gust wind mitigation measurement and control system hardware structure block diagram

The main control chip model in the main control unit is STM32H743, which mainly undertakes the functions of signal processing, data computing and rudder control. The data acquisition module consists of Analog to Digital Converters (ADC), whose main function is to sample the analog signal output from the aeroelastic analog sensor set and get the digital signal that can be processed by the microcontroller. The serial module consists of three serial interface circuits and serial expansion circuits, whose function is to communicate with the aeroelastic digital sensor group, the on-board digital radio, the flight control, and the inertial group module. Servo 1 is a Maxon motor driven by analog voltage with encoder feedback, whose drive signal is generated by Digital to Analog Converters (DAC) controlled by the master control unit, and the number of motors is ten; Servo 2 is a model servo driven by PWM signals, whose drive signal is generated by the master control unit The number of servos is 15. Data storage module SD card, whose role is to store the necessary data such as sensor sampling data, control commands, etc.

The system gets the current data of each sensor of the UAV, such as acceleration sensor, angular velocity sensor, dynamic strain gauge, etc., through the data acquisition module and part of the serial port; it communicates with the ground radio and

2022 IEEE International Conference on Unmanned Systems (ICUS) | 978-1-6654-8456-5/22/$31.00 ©2022 IEEE | DOI: 10.1109/ICUS55513.2022.9986549

the flight control system through the special serial port to get the corresponding control commands. Finally, the main control chip solves the control law according to the current UAV flight status and control instructions, so as to control the rudder surface through the rudder control module and realize the stabilization and wind gust mitigation of the UAV.

III. SYSTEM HARDWARE DESIGN

A. Serial Port Module Circuit Design

In order to realize the communication between the master control unit and the serial peripherals, the serial signals need to be converted to TTL levels that can be handled by the microcontroller through the serial interface circuit, specifically including RS-232, RS-422, RS-485 three types of serial ports. As shown in Fig. 1, the serial module includes three independent RS-232 serial ports and nine sensor-type serial ports. In order to save the resources of the main control chip, the system builds a serial port expansion circuit based on the CH438 chip to expand the nine other serial ports.

1) Serial port interface circuit

The signal level value of RS-232 interface is high, usually reaching more than ten volts, which can easily damage the interface chip if used improperly, and its level standard is also incompatible with TTL level. As shown in Fig. 2, the RS-232 interface circuit designed in this system uses the SP3232 chip as the core to realize the RS-232 to TTL level conversion. Normally, the SP3232 is capable of operating at a data rate of 235kbps and can guarantee a data rate of 120kbps under the worst operating conditions.

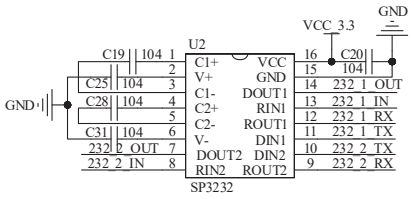

Fig. 2. SP3232-based RS-232 interface circuit diagram

The RS-422 interface has two pairs of twisted pairs, and the transceiver signals do not affect each other, so full duplex communication can be achieved. Each pair of twisted pairs of the interface is in differential form, so it has the ability to suppress common mode interference. As shown in Fig. 3, the RS-422 interface circuit designed for this system uses the MAX3490 chip as the core for RS-422 to TTL level conversion, which is a 3.3V, low-power transceiver for RS-422 communication with a maximum transmission rate of 10Mbps.

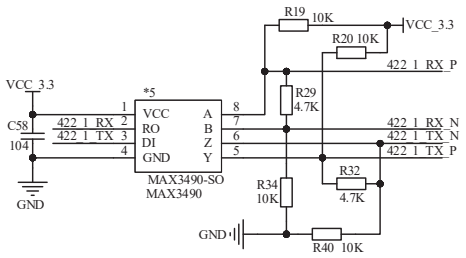

Fig. 3. MAX3490-based RS-422 interface circuit diagram

The RS-485 interface has a pair of twisted pairs, and the transmission and reception cannot be performed simultaneously, so it is a half-duplex communication method. The interface uses balanced transmit and differential receive, which also has the ability to suppress common mode interference. As shown in Fig. 4, the RS-485 interface circuit designed for this system uses the SP485 chip as the core to achieve RS-485 to TTL level conversion. the SP485 is a 3.3V, low-power transceiver for RS-485 communication with a maximum transmission rate of 10Mbps.

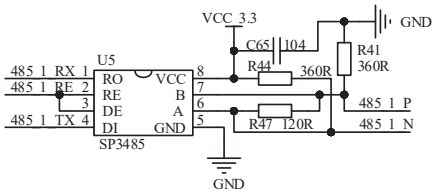

Fig. 4. SP3485-based RS-485 interface circuit diagram

2) Serial port expansion circuit

In order to save the serial port resources of the microcontroller, this system builds a serial port expansion circuit based on the CH438 chip, and the specific structure of the circuit is shown in Fig. 5. In order to increase the serial communication rate, the system achieves a communication rate of 2.7648Mbps by means of an external 22.1184M crystal.

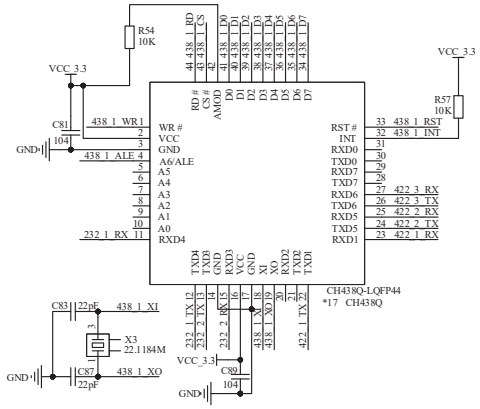

Fig. 5. CH438-based serial port expansion circuit

The system consists of two serial port expansion circuits, which expand a total of nine serial ports. Each serial port expansion circuit is connected to the I/O port of the microcontroller by means of an 8-bit parallel. The serial port signal line in the serial port expansion circuit is connected to the output of the serial port conversion circuit described in the previous section.

B. Signal Sampling Module Circuit Design

The system is based on the ADC circuit of AD7606 to perform analog-to-digital conversion of the analog signal output from the sensor, and the specific circuit structure is shown in Fig. 6. It has the advantages of high signal-to-noise ratio, high noise immunity, high measurement accuracy, low power consumption, etc. It can collect voltage range of ±5V/±10V, sampling rate of 200Ksps, and measurement accuracy of two modes within 0.2mV/0.35mV respectively.

The data acquisition module consists of four ADC circuits based on the AD7606, with 32 signal acquisition channels, each with a different sampling range. The four ADC circuits share a common SPI bus for communication with the microcontroller, and the four AD7606 chips are accessed sequentially through the chip select pins to read the converted data. The OS pins of the AD7606 are oversampling pins, and

the maximum oversampling multiplier of 64x can be achieved through the three oversampling pins. The higher the oversampling multiplier, the slower the conversion speed.

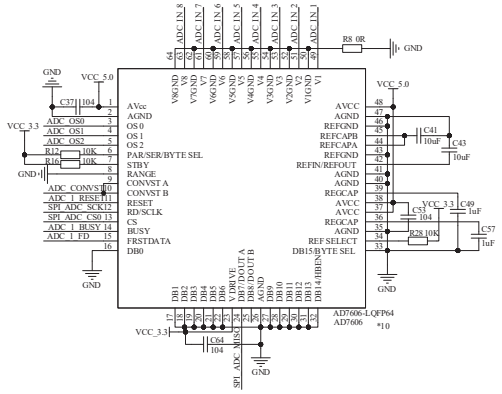

Fig. 6. Analog signal sampling circuit based on AD7606

C. Servo Control Module Circuit Design

As described in *Part II*, the servo control module consists of two types of servos, which are driven by ±10V analog signals and PWM signals, the former of which also has encoder feedback for speed monitoring. Therefore, for Servo 1, the system adopts a DAC circuit based on LTC2688 to realize the ±10V analog signal output and pre-process the feedback signal through the motor encoder feedback circuit to facilitate the capture by the MCU. For Servo 2, the system uses a PCA9685 chip to output 15 PWM waves to drive it.

1) Digital to analog converter circuits

The LTC2688 is a 16-channel, 16-bit, ±10V digital-to-analog converter with an integrated precision reference voltage source and a built-in rail-to-rail output buffer, and the output voltage range of each channel can be programmed independently.

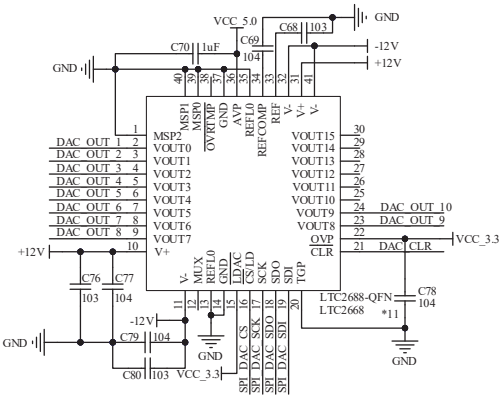

Fig. 7. LTC2688-based digital-to-analog converter circuit

The LTC2688-based DAC circuit is powered by a ±12V supply and is connected to the microcontroller via the SPI interface. The first 10 output channels of the chip are selected as the drive voltage output port of servo 2, and the output voltage has an amplitude range of ±10V.

2) Motor encoder feedback circuit

The servo 1 has an encoder feedback signal, which consists of three phases A, B and Z. Phases A and B are counting phases, and Z is the lap counting phase. The number of pulses in phases A and B is the same when counting, but the phase difference is 90°, and the B phase overrides or lags the A phase to determine whether the servo is in forward or reverse rotation. One pulse in phase Z represents one rotation of the servo. Each phase of the three-phase signal is a differential signal, so a differential signal conversion is required to obtain a single pulse signal.

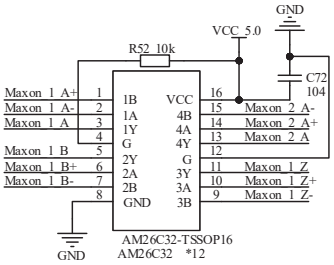

Fig. 8. AM26C32-based encoder feedback circuit

The system builds an encoder feedback circuit based on the AM26C32, the specific structure of which is shown in Fig. 8. The AM26C32 device is a four-way differential line receiver for balanced or unbalanced digital data transmission. The inputs of the circuit are the differential signals of phases A, B and Z, and the outputs are the single pulse signals of each phase.

3) PWM wave output circuit

The driving method of servo 2 is PWM driving, because the number of servos to be driven is large and the timer resources of MCU are limited, so the system is based on PCA9685 to build a PWM signal generation circuit, the specific circuit structure is shown in Fig. 9. PCA9685 is a 12-bit, 16-channel PWM output chip. The chip communicates with the microcontroller through the IIC bus, and the 16-channel PWM wave output can be realized through two wires.

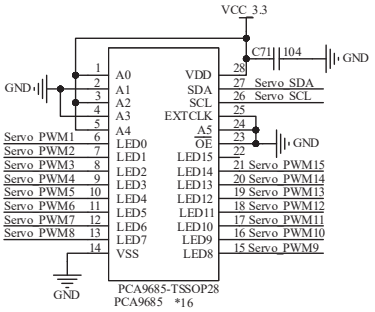

Fig. 9. PWM signal generation circuit based on PCA9685

D. Power Module Circuit Design

The power supply input of the UAV gust wind mitigation measurement and control system is a 2S standard lithium battery with a voltage of 7.4 V. The voltages required by each module of the system are +3.3 V, +5.0 V, +12.0 V, and -12.0 V. Therefore, a DC-DC conversion of the +7.4 V input voltage is required to obtain the above four voltages.

As shown in Fig. 10(a)(b), the +3.3V and +5.0V voltages are generated based on the LM2596, and the input voltage for both circuits is an external +7.4V input. The LM2596 is a linear regulator with inputs up to 37V, and requires few peripheral devices to obtain a stable voltage output. Voltages of +3.3V and +5.0V can be obtained with its submodels LM2596-3.3 and LM2596-5.0.

Fig. 10(c) shows the LT8580-based +5.0V to +12.0V voltage conversion circuit, where +5.0V is the output voltage

of the circuit in Fig. 11(a). The LT8580 is a PWM DC/DC converter containing an internal 1A, 65V switch. The LT8580 has an adjustable oscillator, set by a resistor from the RT pin to ground. The output voltage V_{out} of the circuit is determined by the resistor R_{FBX} connected to the FBX pin, and its specific relationship can be expressed as:

$$R_{FBX} = \frac{V_{out} - 1.204V}{83.3\mu A} \tag{1}$$

A +12.0V to -12.0V voltage conversion circuit based on the TPS5430 is shown in Fig. 10(d), where +12.0V is the voltage output from the circuit in Fig. 10(c). Considering the output of the TPS5430 as ground, the ground side of the circuit is negative. The voltage feedback pin VENSE of the chip is a standard voltage of 1.221V. The corresponding output voltage V'_{out} can be obtained by adjusting the ratio of the two feedback resistors connected to this pin, and the specific calculation relationship can be expressed as:

$$V_{VENSE} = V'_{out} \times \frac{R_1}{R_1 + R_2} \tag{2}$$

Where R_1 is the resistance between the VENSE pin and the output, and R_2 is the resistance between the VENSE pin and the ground.

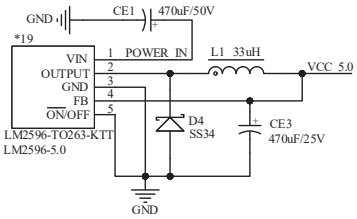

(a) LM2596-based +5.0V voltage regulator circuit

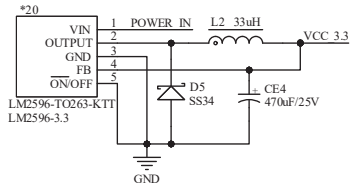

(b) LM2596-based +3.3V voltage regulator circuit

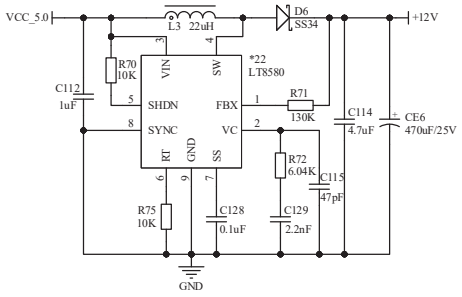

(c) LT8580-based +12.0V voltage regulator circuit

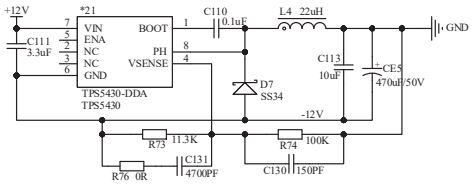

(d) TPS5430-based -12.0V voltage regulator circuit

Fig. 10. Power conversion circuit

E. System Hardware Circuit Fabrication

The physical diagram of the hardware design of the UAV gust wind mitigation measurement and control system is shown in Fig. 11. The circuit board of the system designed in this paper is divided into three parts: the main board composed of the main control unit, the power board composed of four power modules, and the bottom board composed of five other modules. The main board is connected to the base board by means of pins, the power supply board is connected to the base board by four sets of power cables, and the base board is connected to each peripheral through the DB interface.

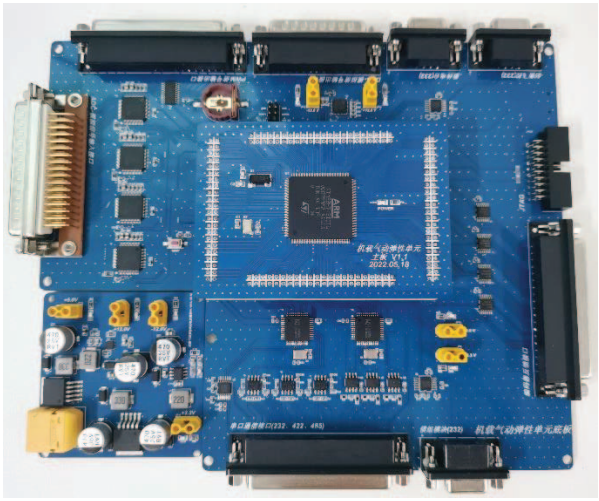

Fig. 11. System hardware design physical diagram

IV. System Software Design

A. Overall Software Architecture

The software design of the system is mainly the program design of the microcontroller, and its program design flow is shown in Fig. 12. After entering the main function, the system clock initialization is carried out first, and then each peripheral circuit is initialized, such as ADC circuit, DAC circuit, serial port expansion circuit, etc. After that, the initialization of SD card, timer and serial port is performed in turn, and finally it enters the dead loop to wait for the arrival of input capture interrupt, serial port interrupt and timer interrupt.

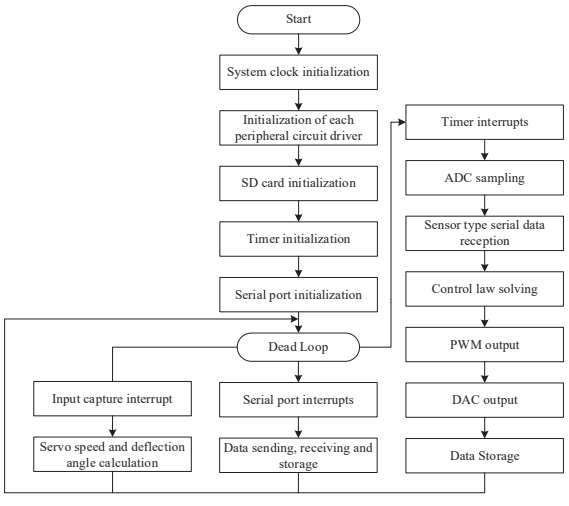

Fig. 12. Microcontroller program design flow chart

The input capture interrupt is triggered when the encoder feedback signal jumps, and the pulse of the encoder feedback

signal is counted after entering this interrupt to obtain the deflection direction and angle of the servo. The serial port receive interrupt is triggered when three independent serial ports receive characters, which will enter the serial port interrupt service function to store and process the serial data. Since the sensor data is required every 10ms for the control law decoding, the system is set to enter the timing interrupt every 10ms to complete the ADC sampling, sensor-like serial port data reception, control law decoding, PWM output, DAC output, and data storage in turn.

B. Serial Module Interface Programming

1) Standalone serial port programming

The system has three independent serial ports directly connected to the microcontroller, and all three serial ports use asynchronous communication method. The serial port transmitting and receiving of the microcontroller are done by two different registers, USART_TDR register for sending data and USART_RDR register for receiving data.

The serial port needs to write the data to be sent to USART_TDR register by calling the standard library function of serial data sending, and wait for the successful sending of data by reading the status of the sending data register.

The execution flow of the receive interrupt of the serial port is shown in Fig. 13. After receiving a character, it enters the serial interrupt service function, then judges the reason of the current interrupt generated, and after confirming that it is a serial receive interrupt, it reads the characters in the USART_RDR register in turn and enters the callback function to process the data and wait for the next interrupt.

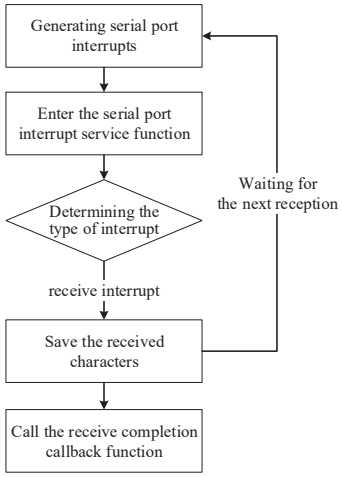

Fig. 13. Serial port receive interrupt execution flow

It is worth noting that the microcontroller needs to agree on the data frame transmission format when communicating with the peripheral device through the serial port, so that both parties can communicate smoothly.

2) Serial port expansion circuit driver design

In addition to the three independent serial ports, the system has nine sensor-like serial ports, all of which are connected to the microcontroller through two CH438-based serial expansion circuits. The two serial port expansion circuits communicate with the microcontroller through parallel connection while using multiplexed address method.

The timing diagram of CH438 is shown in Fig. 14. RD means RD# signal is valid and CS# signal is valid, WR# = 1 & RD# = CS# = 0 for read operation. WR means WR# signal is valid and CS# signal is valid, WR# = CS# = 0 for write operation.

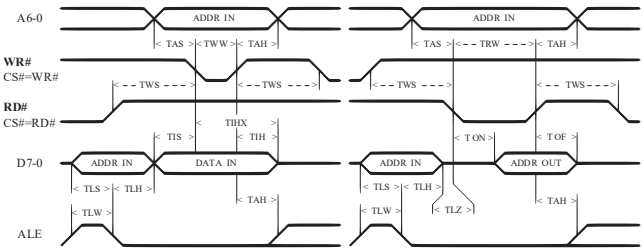

Fig. 14. CH438 timing diagram

When receiving data, first pull the ALE pin high, set the eight-bit parallel I/O port to output mode, write the address to the chip, and select the serial port number. Then pull the ALE pin low, set the eight-bit parallel I/O port to input mode, pull the CS# and RD# pins low, and start reading data. The data received from the serial port shift register RSR is first stored in the receive FIFO and then read out through the receive buffer register RBR. The current reading progress is obtained by reading the DATARDY bit in the line status register LSR, and when this bit is cleared to zero, it means the reading is finished and the data reception of this serial port is completed.

Similar to receiving data, when sending data, the address is first written to the chip, and then the CS# and WR# pins are pulled low to start writing data. The written data is first stored in the transmit FIFO and then output one by one through the transmit shift register TSR. The current reading progress is obtained by reading the THRE bit in the LSR of the line status register, and when this bit is 1, it means that the transmit holding register is cleared and the data transmission of the serial port is completed.

C. Analog-to-digital Converter Circuit Driver Design

The system uses four AD7606 chips for signal sampling. The four chips are mounted to the microcontroller through the SPI bus, and the chip select signal is used to traverse each chip.

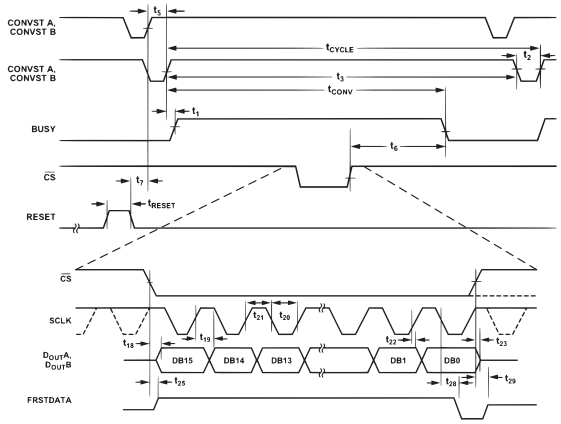

Fig. 15. AD7606 timing diagram

The timing diagram of the AD7606 is shown in Fig. 15. The ADC interface program selects the serial receive mode and starts conversion when a low pulse is received at the CONVST pin, at which time the BUSY pin is automatically pulled high, indicating that the chip is in the conversion phase. During the conversion period, the chip select pin of chip 1 is pulled low to select chip 1 and start reading the converted data. When reading data, eight channels of data are read

sequentially on the $D_{OUT}A$ pin according to the clock signal, with two bytes of data for each channel. After all the data is read, pull up the chip select pin to end the reading process of chip 1.

Similar to the read process of chip 1, after chip 1 is read, a low pulse is given to the CONVST pin again to start a new conversion, and then the chip select pin of chip 2 is pulled low for data reading. Repeat this process until all four chips are read.

D. Servo Control Module Interface Program Design

1) Digital-to-analog converter circuit driver design

The system uses the LTC2688 to build a DAC circuit to generate ten analog voltage signals in the range of -10V to +10V to drive the servo 1 for the corresponding angle of deflection. each output channel of the LTC2688 can be programmed independently.

The timing diagram of the LTC2688 is shown in Fig. 16. Before writing data, first pull the $\overline{CS}$/LD pin low to enable the chip. Then the data to be sent through the SDI pin at the rising edge of the clock (SCK pin) is loaded into the shift register. First, 4-bit command C3-C0 is loaded to configure the write range and other operations; then 4-bit DAC address A3-A0 is loaded to select output channel 1; finally, a 16-bit data word in direct binary format is loaded, and the value of the data word represents the magnitude of the output voltage value. After completing the output voltage setting of chip 1, keep the $\overline{CS}$/LD pin low, transfer the 24-bit input word again, and select output channel 2 for output voltage setting. Repeat this process until all ten channels are set, and then pull the $\overline{CS}$/LD pin high to complete the entire DAC output setting process.

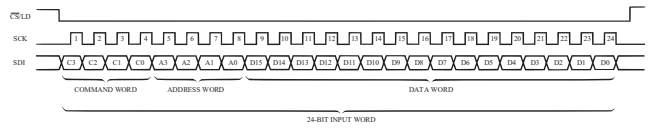

Fig. 16. LTC2688 timing diagram

2) PWM Generator Driver Design

The system uses the PCA9685 to generate 15 PWM waves to drive the servo 2 for deflection. The deflection angle of the servo can be controlled by adjusting the duty cycle of the PWM waveform. In the PWM control function, the IIC bus is used to write the address of each channel in turn using the standard HAL library function to select the output channel and set the PWM frequency and duty cycle.

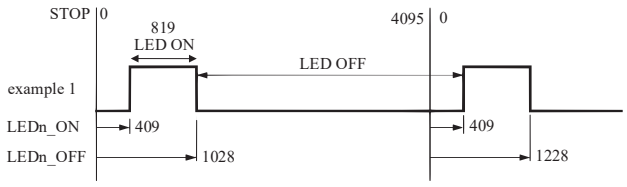

Fig. 17. Diagram of PWM duty cycle setting method

The PCA9685 PWM duty cycle size for each channel is set in the way shown in Fig. 17. The PWM duty cycle of each output channel can be controlled independently using the LEDn_ON and LEDn_OFF registers, where n represents the number of the output channel and ranges from 0 to 15. The size of LED ON in the figure is the value of the LEDn_OFF register minus the value of the LEDn_ON register, and the size of LED OFF is 4096 minus the value of LED ON. Then the output PWM wave duty cycle V_{DC} can be expressed as:

$$V_{DC} = \frac{V_{LEDn\_OFF} - V_{LEDn\_ON}}{4096} \times 100\% \tag{3}$$

where V_{LEDn_ON} is the value in the LEDn_ON register, V_{LEDn_OFF} is the value in the LEDn_OFF register, and n is the number of the output channel.

In actual use, the value of V_{LEDn_ON} is set to 0, then the duty cycle can be set by modifying the size of V_{LEDn_OFF} value.

The PWM output frequency of PCA9685 is set by register PRE_SCALE, and the relationship between the value of PRE_SCALE and PWM output frequency can be expressed as follows:

$$prescale\ value = round\left(\frac{osc\_clock}{4096 \times update\_rate}\right) - 1 \tag{4}$$

Where osc_clock is the clock frequency of the oscillator and $update\_rate$ is the PWM frequency to be set.

V. Experiments and Analysis

After the hardware circuit design and microcontroller software design, each of the four circuit modules described in Part III was tested and analyzed to verify its viability as a gust mitigation measurement and control system.

A. Serial Module Testing and Analysis

For the serial module, the serial interface circuit is relatively simple, now mainly test the serial expansion circuit based on CH438. The serial expansion circuit is connected to a PC, and the PC's serial debugging assistant is used to send a frame of data to the measurement and control system, which then sends it back after receiving it. The data format of each byte is set to 8 data bits, one stop bit and no parity bit.

After actual testing, the number of bytes received was the same as the number of bytes sent after about 10 million bytes had been sent from the PC, i.e. no packet loss occurred during the communication process and the transmission process was stable. This is because the CH438's data reception FIFO is a maximum of 112 bytes, and when the size of the frames sent by the sender exceeds this amount, the FIFO overflows and cannot be received correctly. This is due to the limitations imposed by the hardware characteristics and the frame size of the connected device should be taken into account when using the CH438 in order to avoid data loss.

B. Signal Sampling Module Testing and Analysis

The signal sampling module mainly consists of an ADC circuit, whose function is to perform an analogue-to-digital conversion of the analogue signals output from each sensor, thus facilitating the main control to perform calculations and obtain the current flight status of the UAV. Therefore, the ADC circuit has to sample the analogue signal output from each sensor as accurately as possible in order to obtain the correct sensor data.

This experiment measures the performance of the ADC circuit by comparing the actual voltage value with the measured voltage value. The sampling range is set to [-10V, +10V], the oversampling multiplier is 4, and the conversion period reading is taken to obtain the analogue-to-digital conversion results. A total of nine sets of data were tested from

-10V to +10V, using 2.5V as the interval, and the results are shown in Table I.

TABLE I. ADC CRCUIT TEST RESULTS

Serial number	Actual voltage(V)	Sampling voltage(V)	Error
1	-10.0	-9.998	0.02%
2	-7.5	-7.505	0.07%
3	-5.0	-5.007	0.14%
4	-2.5	-2.502	0.08%
5	0.0	-0.001	0.10%
6	+2.5	+2.502	0.08%
7	+5.0	+5.004	0.08%
8	+7.5	+7.504	0.05%
9	+10.0	+9.997	0.03%

As can be seen from Table I, the voltage values collected by the ADC sampling circuit are basically the same as the actual voltage values, with overall errors within 0.15% and within 0.1% in the vast majority of cases. In the case of low sampling speed requirements, the sampling accuracy can be further improved by increasing the oversampling multiplier. Therefore, the system can sample the analogue signal in real time and accurately, so as to obtain accurate UAV status information.

C. Servo Control Module Testing and Analysis

1) Digital to analogue converter circuits

The output of the DAC module is an analogue voltage in the range [-10V, +10V], which controls the speed and direction of rotation of the motor by the magnitude and polarity of the voltage. It is therefore important that the output voltage is accurate in order to allow the motor to rotate at the specified angle as instructed by the system, thus achieving the desired wind gust mitigation effect. This experiment measures the performance of the DAC circuit by comparing the difference between the actual voltage value and the set voltage value. 9 sets of data were tested and the results are shown in Table II.

TABLE II. DAC CIRCUIT TEST RESULTS

Serial number	Setting voltage(V)	Output voltage(V)	Error
1	-10.0	-9.999	0.01%
2	-7.5	-7.497	0.04%
3	-5.0	-5.001	0.02%
4	-2.5	-2.499	0.04%
5	0.0	0.000	0.0%
6	+2.5	2.499	0.04%
7	+5.0	5.001	0.02%
8	+7.5	7.498	0.03%
9	+10.0	10.001	0.01%

As can be seen from Table II, the output voltage magnitude of the DAC circuit is basically the same as the set value, and the error between the two is within 0.05%, which meets the driving accuracy requirement of the corresponding servo. This shows that the DAC circuit designed in this paper can complete the analog-to-digital conversion very well, laying the foundation for accurate gust mitigation.

2) PWM output circuit

The PWM output circuit is used to control the deflection of a PWM driven servo, which requires a fixed PWM frequency of 50 Hz and deflects the corresponding angle by the duty cycle. This experiment measures the performance of the PWM output circuit by comparing the actual PWM duty cycle output with the set duty cycle. 5 sets of data were tested and the results are shown in Table III.

TABLE III. PWM OUTPUT CIRCUIT TEST RESULTS

Serial number	Setting Duty Ratio	Output Duty Ratio
1	0.0%	0.0%
2	25.0%	25.1%
3	50.0%	49.8%
4	75.0%	74.9%
5	100.0%	100.0%

As shown in Table III, the PWM duty cycle output of the tested circuit is consistent with the actual duty cycle set, with a maximum error of 0.2%, allowing for accurate control of the servo. The output PWM frequency was also measured to be 50.01Hz, which meets the driving frequency requirements of the servo.

D. Power Module Testing and Analysis

The accuracy and stability of the output voltage of the power supply module is the basis and guarantee of the stable operation of the entire circuit system. The power supply module in this system has four outputs, which supply power to different parts of the system. This experiment tests the stability of the power supply module by testing its output voltage under different voltage inputs. A total of three sets of data were tested and the specific test results are shown in Table IV.

TABLE IV. POWER MODULE TEST RESULTS

Serial number	Module input(V)	Module output(V)			
		+3.3V	*+5.0V*	*+12.0V*	*-12.0V*
1	7.4	+3.276	+5.02	+12.05	-12.06
2	8.5	+3.275	+5.02	+12.05	-12.06
3	11.1	+3.275	+5.02	+12.05	-12.06
Average error		0.74%	0.40%	0.41%	0.50%

As can be seen from Table IV, the output error for all four voltages is within 0.75% and the output voltage of the module remains largely unchanged as the input voltage increases. Of the three sets of data tested, 7.4V and 11.1V represent the lithium battery voltage magnitudes for the 2S and 3S standards respectively. It can be concluded that the power module can be adapted to a wide range of standard voltage inputs, while being able to output an accurate and smooth voltage, ensuring stable system operation.

VI. CONCLUSIONS

This paper develops a UAV gust mitigation measurement and control system based on the STM32H743 microcontroller, and introduces the hardware circuit design and microcontroller software design of the system. After actual circuit fabrication and experimental testing, the system can achieve stable serial communication, accurate analogue signal acquisition, precise motor and servo control and stable power

supply, meeting the required specifications and requirements for gust mitigation. The measurement and control system will be verified in the future by carrying out wind tunnel tests and actual flight tests on an unmanned aircraft platform.

ACKNOWLEDGMENT

This work was supported by the Science and Technology Innovation 2030-Key Project of "New Generation Artificial Intelligence" under Grant 2020AAA0108200.

REFERENCES

[1] L. J. Zhu, X. Z. Yang, J. J. Fan. Constant-Height control system for unmanned aerial vehicle at low altitude aiming at gust disturbance[J]. Computer Application and Software,2020,37(08):79-84.

[2] J. B. Yang, Z. G. Wu, Y. T. Dai, et al. Wind tunnel test of gust alleviation active control for flying wing configuration aircraft[J]. Journal of Beijing University of Aeronautics and Astronautics,2017,43(1):182-192.

[3] C. J. Jin, Y. L. Xiao. Principles of flight in atmospheric disturbances[M]. Beijing: Defense Industry Press,1992.

[4] Y Yang, C Yang, Z. G. Wu. A design of gust alleviation control system based on test of actuator' s dynamic characteristics[J]. Journal of Vibration and Shock,2020,39(04):106-112.

[5] J. E. Cooper, I. Chekkal, R. C. M. Cheung, et al. Design of a morphing wingtip[J]. Journal of Aircraft, 2015,52(5):1394-1403.

[6] L. O. Bernhammer, S. P. W. Teeuwen, R. De Breuker; Gust load alleviation of an unmanned aerial vehicle wing using variable camber[J], Journal of Intelligent Material Systems and Structures, 2014,25(7):795-805.

[7] J Copper, S Miller, O Sensburg, et al. Optimization of a scaled sensorcraft model with passive gust alleviation[C]/12th AIAAISSMO Multdisciplinary Analysis and Optimization Conference.Reston:AIAA,2008.

[8] Y. T. Zhou, Y. Yang, Z. G. Wu, C. Yang. Flight test for gust alleviation on a high aspect ratio UAV platform[J]. Journal of Aeronautics, 2022,43(06):326-337.